ELSEVIER

1 October 1996

Optics Communications 130 (1996) 288–294

OPTICS COMMUNICATIONS

Higher-order space charge field effects on the evolution of spatial solitons in biased photorefractive crystals

S.R. Singh, M.I. Carvalho, D.N. Christodoulides

Department of Electrical Engineering and Computer Science, Lehigh University, Bethlehem, PA 18015, USA

Received 21 February 1996; revised version received 18 April 1996; accepted 18 April 1996

Abstract

We investigate higher-order space charge field effects on the evolution of bright spatial solitons in biased photorefractive crystals under steady-state conditions. Numerical simulations demonstrate that these optical solitons can experience considerable increase in their self-deflection especially in the regime of very high bias field strengths. This process is further studied using perturbation techniques. Our analysis indicates, that for very high bias fields, the self-bending process is further enhanced by a factor that varies cubically with the applied field. Relevant examples are provided.

Lately, spatial optical solitons in photorefractive (PR) materials have been a topic of considerable research [1–6]. Of particular interest are the so-called screening solitons which are possible in steady-state when an external bias voltage is appropriately applied to a PR crystal [2,3]. Thus far, bright, dark and gray steady-state domains have been predicted. These soliton states occur provided the bias field is relatively high so that the drift term dominates in the expression of the space charge field. In a recent study [7], the effects arising from first-order diffusion terms have been investigated. In particular, it was found that the PR soliton can experience adiabatic self-deflection which varies linearly with the applied electric field. However, recent experiments [8] have shown that this self-deflection can exceed the one predicted by theory [7], especially in the regime of quite high bias fields.

To account for this discrepancy, we here investigate the effects arising from other higher-order space charge field terms on the evolution of bright steady-state solitons in PR media. Our numerical results indicate that these optical solitons experience considerable increase in their self-deflection especially in the regime of very high bias field strengths. Moreover, we find that these spatial beams remain approximately invariant during propagation. The self-bending process is further studied using perturbation procedures which involve the conservation laws of the nonlinear wave equation. Our analysis predicts that the optical beam moves on a parabolic trajectory and that the central spatial frequency component shifts linearly with the propagation distance. Unlike the low bias field case in which the process is dominated by first-order diffusion effects [7], in the high bias regime the self-deflection is found to be enhanced by a factor which varies cubically with the applied field strength. These analytical results are then compared to those obtained numerically and are found to be in good agreement.

To start, let us first consider an optical beam that propagates in a PR crystal along the z-axis and is

PII S0030-4018(96)00288-X

allowed to diffract only along the x direction. For demonstration purposes, the PR material is taken here to be strontium barium niobate (SBN) [9] with its optical c-axis oriented along the x coordinate. Moreover, let us assume that the optical beam is linearly polarized along x and that the external bias electric field is applied in the same direction. Under these conditions, the perturbed extraordinary refractive index is given by $n_e'^2 = n_e^2 - n_e^4 r_{33} E_{sc}$ [10] where r_{33} is the electrooptic coefficient involved, n_e is the unperturbed extraordinary index of refraction and $\boldsymbol{E}_{sc} = E_{sc}\hat{x}$ is the induced space-charge field. Following Ref. [3], the induced space-charge electric field can be directly obtained from the Kukhtarev-Vinetskii model [11] and is given by

$$E_{sc} = E_0 \frac{I_d}{I+I_d}\left(1 + \frac{\epsilon_0\epsilon_r}{eN_A}\frac{\partial E_{sc}}{\partial x}\right) - \frac{K_B T}{e}\frac{(\partial I/\partial x)}{(I+I_d)} + \frac{K_B T}{e}\frac{\epsilon_0\epsilon_r}{eN_A}\frac{\partial^2 E_{sc}}{\partial x^2}, \tag{1}$$

where $I = I(x,z)$ is the power density of the optical beam and it is related to the slowly varying envelope ϕ through Poynting's vector, i.e. $I = (n_e/2\eta_0)|\phi|^2$. In Eq. (1), I_d is the dark irradiance, e is the electron charge, N_A is the acceptor density and ϵ_r is the static relative permittivity. E_0 represents the value of the electric field in the dark regions (at $x \to \pm\infty$) of the crystal. If the spatial extent of the optical wave is much less than the x-width W of the PR sample, then under a constant voltage bias V, E_0 is approximately given by V/W [3]. In obtaining Eq. (1), it was also implicitly assumed that the optical beam involved is of the bright type [3]. At moderately high bias voltage, V, the space charge field, E_{sc}, is heavily dominated by drift and moreover in typical PR materials the dimensionless quantity $|(\epsilon_0\epsilon_r/eN_A)\partial E_{sc}/\partial x| \ll 1$. In that case, to first order, E_{sc} is approximately given by [2,3]

$$E_{sc} \approx E_{sc_0} = E_0 \frac{I_d}{I+I_d}. \tag{2}$$

Note, that the term $(\epsilon_0\epsilon_r/eN_A)\partial E_{sc}/\partial x$ indicates the extent by which the ionized donor density, N_D^+, deviates locally from the trap density N_A [3]. To study the effects arising from higher-order space charge field terms such as $\partial E_{sc}/\partial x$ and $\partial^2 E_{sc}/\partial x^2$ in Eq. (1), we now use the first-order solution of Eq. (1), i.e. Eq. (2), and in turn the other terms are obtained in an iterative fashion. By doing so, the perturbative solution of the space charge field, E_{sc}, reads as follows:

$$E_{sc} = E_{sc_0} + E_{\gamma_1} + E_{\gamma_2} + E_{\gamma_3} + E_{\gamma_4}, \tag{3}$$

where

$$E_{\gamma_1} = -\frac{K_B T}{e}\frac{(\partial I/\partial x)}{(I+I_d)},$$

$$E_{\gamma_2} = -\frac{\epsilon_0\epsilon_r}{eN_A}\frac{E_0^2 I_d^2}{(I+I_d)^3}\left(\frac{\partial I}{\partial x}\right),$$

$$E_{\gamma_3} = \frac{2K_B T}{e}\frac{\epsilon_0\epsilon_r}{eN_A}\frac{E_0 I_d}{(I+I_d)^3}\left(\frac{\partial I}{\partial x}\right)^2,$$

$$E_{\gamma_4} = -\frac{K_B T}{e}\frac{\epsilon_0\epsilon_r}{eN_A}\frac{E_0 I_d}{(I+I_d)^2}\left(\frac{\partial^2 I}{\partial x^2}\right). \tag{4}$$

It is important to note that Eq. (3) is valid as long as the perturbations E_{γ_i} $(i = 1, 2, 3, 4)$ are much smaller than the leading term of the space charge field, E_{sc_0}. The envelope propagation equation is then obtained by substituting the expression for the perturbed refractive index (induced by the space charge field) into the paraxial wave equation [3]. After appropriate normalizations, the envelope U is then found to obey the following dynamical evolution equation:

$$iU_\xi + \frac{U_{ss}}{2} - \beta\frac{U}{1+|U|^2} + \gamma_1\frac{(|U|^2)_s U}{1+|U|^2} + \gamma_2\frac{(|U|^2)_s U}{(1+|U|^2)^3} - \gamma_3\frac{[(|U|^2)_s]^2 U}{(1+|U|^2)^3} + \gamma_4\frac{(|U|^2)_{ss} U}{(1+|U|^2)^2} = 0, \tag{5}$$

where $U = [n_e/(2\eta_0 I_d)]^{1/2}\phi$, i.e. the power density is normalized with respect to the dark irradiance $(I/I_d = |U|^2)$, and $U_\xi = \partial U/\partial\xi$, etc. The dimensionless transverse coordinate s is given by $s = x/x_0$, where x_0 is an arbitrary spatial scale, and the normalized coordinate ξ is related to the actual propagation distance z through $\xi = z/(k_0 n_e x_0^2)$, where

$k_0 = 2\pi/\lambda_0$ is the free space wavevector. The dimensionless quantity β is associated with the process of drift and is equal to $\beta = (k_0 x_0)^2 (n_e^4 r_{33}/2) E_0$. In Eq. (5), the γ_1 term represents the first-order diffusion process whereas γ_2, γ_3 and γ_4 are higher order space charge field effects. Note, that the γ_2 term primarily arises from the deviation of N_D^+ from N_A. The γ coefficients are given by $\gamma_1 = \beta\delta$, $\gamma_2 = \beta\epsilon E_0^2$, $\gamma_3 = 2\beta\delta\epsilon E_0^2$, $\gamma_4 = \beta\delta\epsilon E_0^2$ where $\delta \equiv (K_B T/e x_0 E_0)$ and $\epsilon \equiv (\epsilon_0 \epsilon_r / E_0 x_0 e N_A)$. It is also important to note that the fundamental soliton solutions of Eq. (5) are obtained by considering only the drift nonlinearity (i.e. the β term) and by neglecting all the γ-perturbations [2,3]. These planar bright solitons are only possible when β or E_0 are positive quantities. As previously shown, the intensity full width half maximum (FWHM) of these solitary beams depends only on two parameters namely E_0 and r [2,3]. The positive ratio r is defined as $r \equiv I_{max}/I_d$, where I_{max} is maximum power density of the solitary beam. Finally, the following remark may be necessary in order to better understand the anticipated role of these γ-perturbations. From Eq. (5), it is clear that the γ_1 and γ_2 terms will have odd effects (such as beam-deflection) on an otherwise even in x spatial beam whereas the γ_3 and γ_4 are expected to produce an even perturbation such as spatial broadening.

We will now investigate the effects arising from these higher-order γ terms on such bright soliton states. By assuming solitary wave solutions as input beam profiles, Eq. (5) is solved numerically using a beam propagation method. As an example, let us consider a SBN:60 PR crystal with the following parameters [9]: $n_e = 2.33$, $r_{33} = 237$ pm/V, $N_A = 4 \times 10^{16}\text{cm}^{-3}$ and $\epsilon_r = 880$. Moreover, the free space wavelength, λ_0, is taken here to be 0.5 μm. If we let the arbitrary spatial scale, x_0, be 25 μm and the bias field $E_0 = 1$ kV/cm, we find that $\beta = 34.5$, $\gamma_1 = 0.35$, $\gamma_2 = 0.168$, $\gamma_3 = 0.0035$ and $\gamma_4 = 0.0017$. By solving Eq. (5), we find that the optical soliton experiences adiabatic self-deflection and moves approximately on a parabolic trajectory. On the other hand its power spectrum shifts linearly with propagation distance. Figs. 1(a) and (b) depict the evolution of an $r = 10$ soliton and its power spectrum respectively at $E_0 = 2$ kV/cm. In this case, the spatial and angular shifts are considerably higher than those

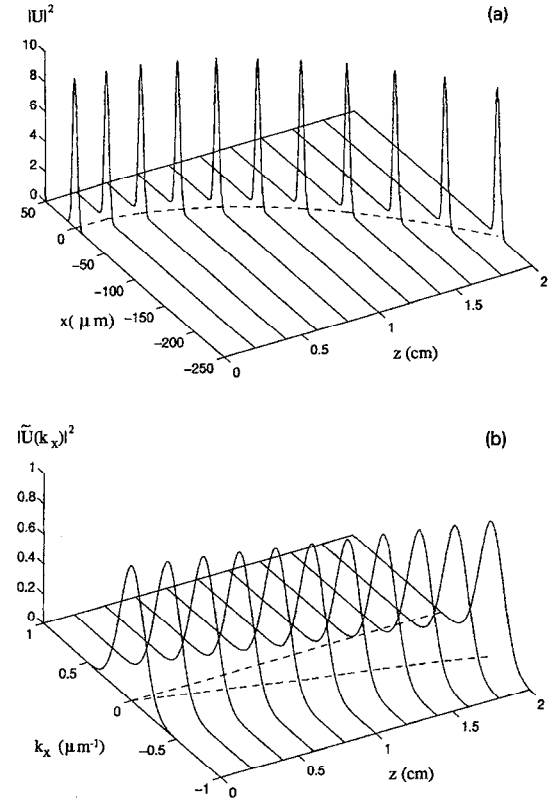

Fig. 1. Evolution of (a) the intensity profile and (b) the angular power spectrum of an $r = 10$ soliton at $E_0 = 2$ kV/cm under the influence of γ_1 and γ_2 terms.

previously obtained [7] by considering the first-order diffusion term, γ_1, alone. This effect is more pronounced at higher applied electric field strengths. Fig. 2(a) compares the spatial self-deflection due to γ_1 alone to that obtained when both γ_1 and γ_2 act together at different applied electric field strengths of E_0, i.e. $E_0 = 1$, 2 and 5 kV/cm. A fundamental bright soliton with $r = 3$ is used at the input. It is quite clear from the figure that at low bias fields the process is dominated by first-order diffusion effects whereas at high bias fields one needs to account for γ_2 effects. These results support the experimental observations of Ref. [8]. This increasing effect of the γ_2 term with E_0 becomes more evident by looking at the corresponding perturbations in the space charge field. Fig. 2(b) compares the various space charge field contributions (normalized with respect to E_0) i.e E_{sc_0}/E_0 and E_{γ_i}/E_0 ($i = 1, 2, 3, 4$), at these

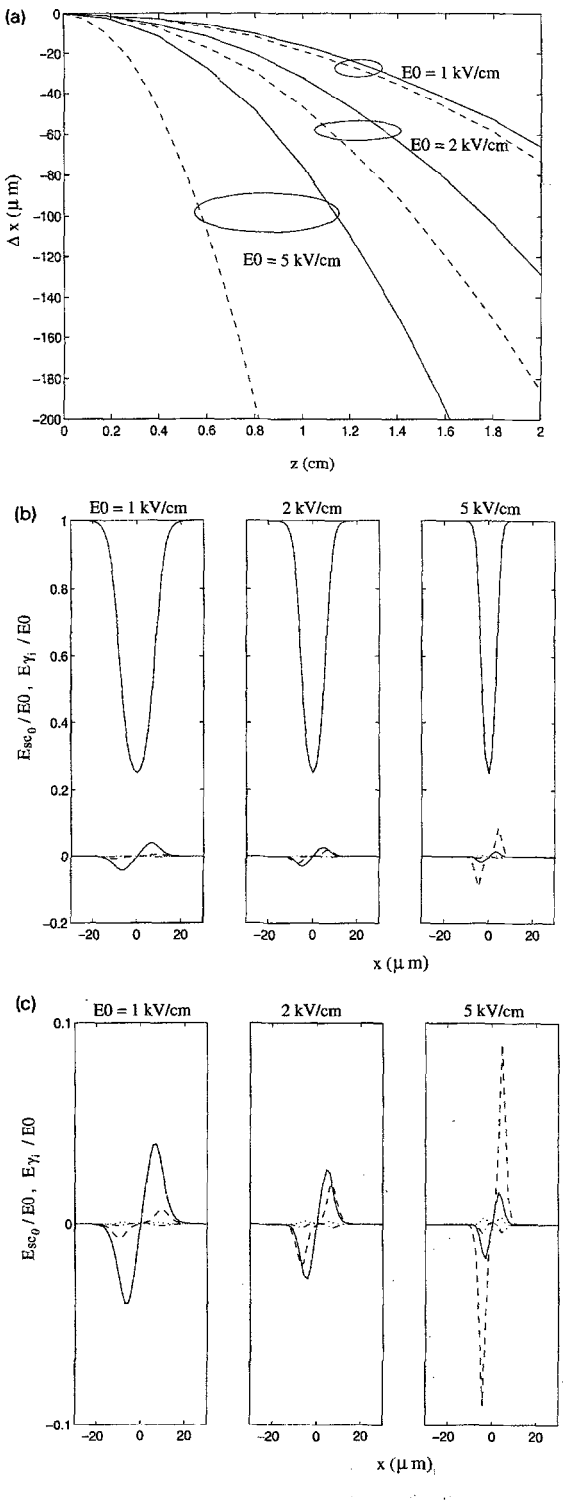

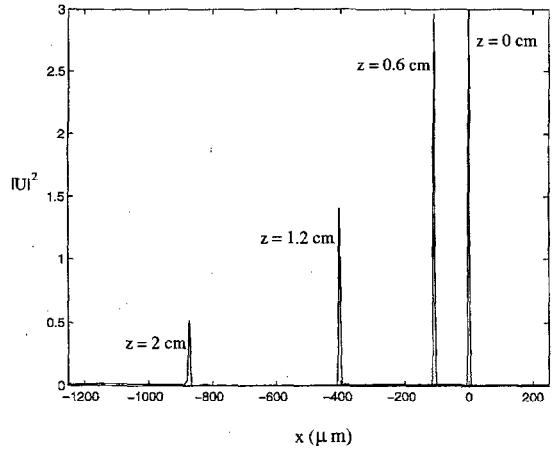

Fig. 3. Intensity profiles of an $r = 3$ soliton input beam at $z = 0$, 0.6, 1.2 and 2 cm at $E_0 = 5$ kV/cm.

three values of E_0, that is $E_0 = 1$, 2 and 5 kV/cm. The perturbations, $E_{\gamma_{1,2,3,4}}/E_0$, have been enlarged in Fig. 2(c) for convenience. Figs. 2(b) and 2(c) indicate that these perturbations are small compared to the leading term, E_{sc_0}. At $E_0 = 1$ kV/cm, E_{γ_1} is the dominant second order contribution whereas E_{γ_2} is still rather small. However, E_{γ_2} tends to increase rapidly at higher values of E_0. For example, at $E_0 = 5$ kV/cm its contribution becomes quite large and dominates over the other terms and the perturbative approach of Eq. (3) is now reaching its limits. It is also interesting to note that at such high bias fields, the soliton is found to rapidly lose its amplitude and form after a certain distance of propagation. Fig. 3 shows the intensity profiles of an $r = 3$ soliton input beam at various distances of $z = 0$, 0.6, 1.2 and 2 cm at $E_0 = 5$ kV/cm. As one can see, the intensity of the optical beam reduces from 3 at the

Fig. 2. (a) Comparison of spatial shifts obtained by considering the γ_1 term alone (solid curve) and the γ_1, γ_2 terms together (dashed curve). (b) Plots of various normalized electric field contributions, E_{sc_0}/E_0 and $E_{\gamma_{1,2,3,4}}/E_0$ where the main lobe represents E_{sc_0}/E_0 and the small contributions around the zero line are the E_{γ_i}/E_0 terms. (c) An expanded view of the perturbations E_{γ_1}/E_0 (solid curve), E_{γ_2}/E_0 (dashed curve), E_{γ_3}/E_0 (dotted curve) and E_{γ_4}/E_0 (dashed-dot curve). All the plots have been calculated at three different applied electric field strengths of $E_0 = 1$, 2, and 5 kV/cm. A fundamental bright soliton with $r = 3$ is used at the input.

input to less than 1 after 1.4 cm of propagation. Moreover, its intensity FWHM increases from 5 μm to 8 μm, that is by 60%, at $z=2$ cm. If E_0 is increased further, this process is reached earlier. Nevertheless, in the regime in which the soliton evolution is still adiabatic, one can use perturbative procedures to treat this self-deflection process. It is also important to note that, for the range of applied electric fields below 5 kV/cm, the γ_3 and γ_4 terms were not found to have any significant effects. Since they play a negligible role, they will be omitted in our analysis from this point on.

The self-bending effect will now be further investigated using perturbative procedures [7]. Keeping in mind that the beam evolution is approximately adiabatic, we start by making the following ansatz for the solution of Eq. (5):

$$U = r^{1/2} y[s + \nu(\xi)] \times \exp\{i[\mu\xi + w(\xi)(s + \nu(\xi)) - \alpha(\xi)]\}, \tag{6}$$

where $U(\xi,s) = r^{1/2} y(s) \exp(i\mu\xi)$ is the steady-state fundamental bright soliton solution of Eq. (5) when all the γ terms are neglected. In Eq. (6), $\nu(\xi)$ represents a shift in the position of the beam center, $w(\xi)$ is associated with the angle between the central wavevector of this beam and the propagation axis ξ, and $\alpha(\xi)$ is the phase accumulated during propagation. The equations of motion of these real variables can then be obtained by substituting Eq. (6) into the two complex conservation laws of Eq. (5) [7,12,13] when γ_3 and γ_4 are equal to zero. By doing so, a straightforward calculation yields the following results: $d\nu/d\xi = -w$, $d\alpha/d\xi = -w^2/2$ and $dw/d\xi = 4\beta[\gamma_1 K_1(r) + \gamma_2 K_2(r)]$, where the dimensionless functions $K_{1,2}(r)$ are given by

$$K_{1,2}(r) = \left(\int_{-\infty}^{+\infty} ds \frac{2y^2(s)}{[1 + ry^2(s)]^{1,3}} \times \{y^2(s)\ln(1+r) - \ln[1 + ry^2(s)]\} \right) \times \left(\int_{-\infty}^{+\infty} ds\, y^2(s) \right)^{-1}. \tag{7}$$

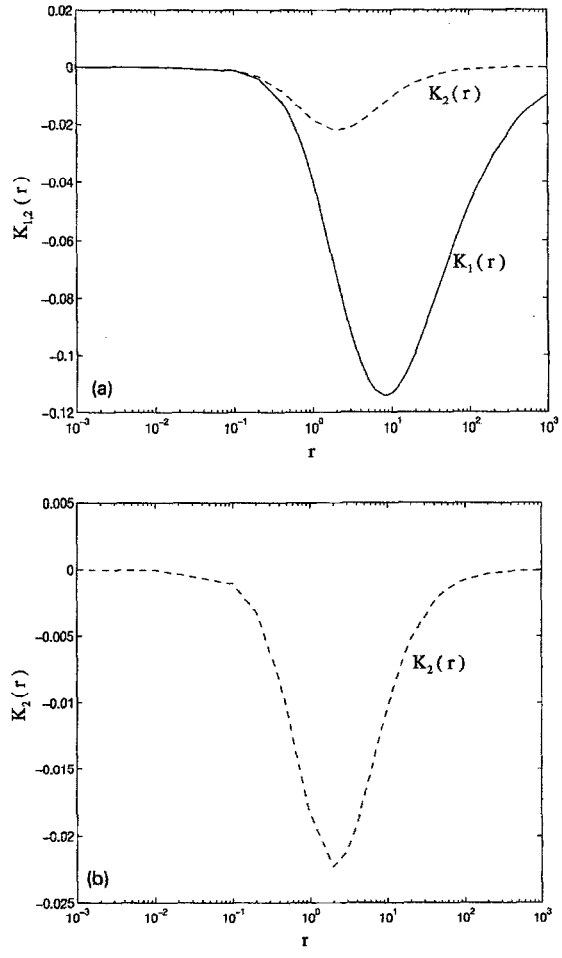

Fig. 4. (a) Dependence of K_1 (solid curve) and K_2 (dashed curve) functions on r and (b) an expanded view of the $K_2(r)$ function.

Note that the exponent power of the term $[1 + ry^2(s)]$ is 1 in obtaining $K_1(r)$ [7] whereas is 3 in the case of $K_2(r)$. These functions are uniquely determined by the value of the parameter r. In the low amplitude soliton regime, that is for $r \ll 1$, K_1 and K_2 can be directly obtained by substituting the low amplitude beam solution [3] of Eq. (5), i.e. $y(s) = \mathrm{sech}[(\beta r)^{1/2} s]$, when $\gamma_i = 0$ into Eq. (7). In this case, $K_1(r) \approx K_2(r) \approx -(2r^2/15)$. However, for other values of r these functions can only be evaluated numerically. Their behavior as a function of r is depicted in Fig. 4(a). The function $K_2(r)$ is also shown on an expanded scale in Fig. 4(b). The equa-

tions of motion for w, ν and α can then be directly integrated, in which case we obtain:

$$w(\xi) = 4\beta[\gamma_1 K_1(r) + \gamma_2 K_2(r)]\xi, \tag{8}$$

$$\nu(\xi) = -2\beta[\gamma_1 K_1(r) + \gamma_2 K_2(r)]\xi^2, \tag{9}$$

$$\alpha(\xi) = -8\{\beta[\gamma_1 K_1(r) + \gamma_2 K_2(r)]\}^2(\xi^3/3). \tag{10}$$

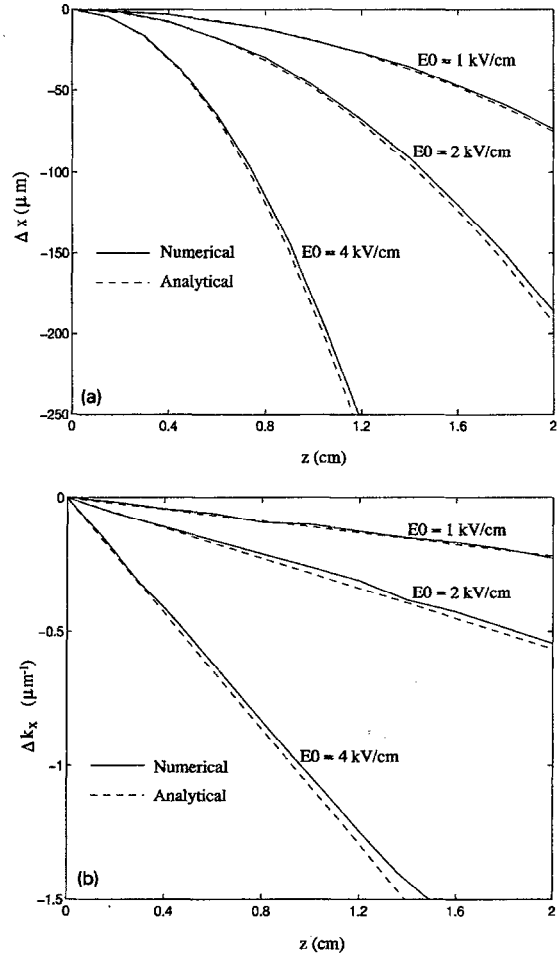

Fig. 5. Evolution of (a) the spatial shift, Δx, and (b) the angular power spectrum shift, Δk_x, obtained from the numerical solution (solid line) and the analytical model (dashed line). Comparison is made at different applied electric field strengths of $E_0 = 1$, 2 and 4 kV/cm. A fundamental bright soliton with $r = 3$ is used at the input. Both γ_1 and γ_2 terms are considered.

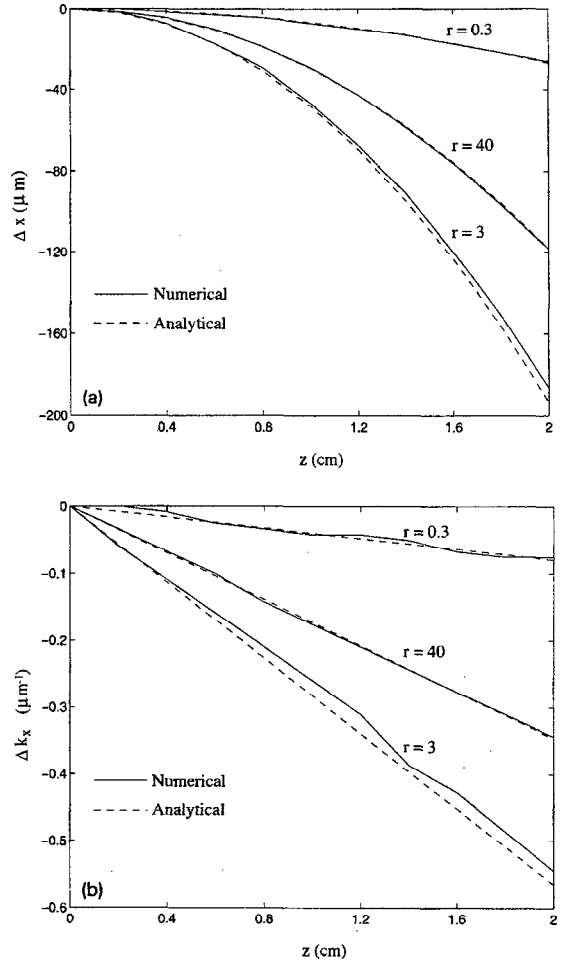

Fig. 6. Evolution of (a) the spatial shift, Δx, and (b) the angular power spectrum shift, Δk_x, obtained from the numerical solution (solid line) and the analytical model (dashed line). Comparison is made for different values of $r = 0.3$, 3 and 40. The soliton solutions were obtained at $E_0 = 2$ kV/cm. Both γ_1 and γ_2 terms are considered.

From these latter results, one quickly finds that the beam suffers a lateral displacement which is given by

$$x_d = \left[\left(k_0 n_e^3 r_{33}\right)^2/2\right]\left[\left(K_B T/e\right)E_0 K_1(r) + \left(\epsilon_0 \epsilon_r / e N_A\right)E_0^3 K_2(r)\right] z^2, \tag{11}$$

where z is the actual propagation distance. The angular deflection i.e. the angle between the central

wavevector of this solitary beam and the z-axis can also be evaluated and is given by

$$\theta_d = \left(k_0 n_e^3 r_{33}\right)^2 \left[\left(K_B T/e\right) E_0 K_1(r) + \left(\epsilon_0 \epsilon_r / e N_A\right) E_0^3 K_2(r)\right] z. \quad (12)$$

Eqs. (9) and (11) clearly demonstrate that the beam center follows a parabolic trajectory, whereas Eqs. (8) and (12) imply that the central spatial frequency component shifts linearly with propagation distance. Moreover, Eqs. (8)–(12) show that in the presence of γ_2, the self-deflection now follows a cubic polynomial of E_0. This implies that self-deflection will increase considerably at higher values of applied field strengths. Similar conclusions were reached by numerically solving Eq. (5). Figs. 5(a) and 5(b) depict both the spatial as well as the angular frequency shift i.e. Δx and $\Delta k_x \equiv w/x_0$ as obtained using both approaches. The shifts experienced by an $r = 3$ soliton are compared at different applied field strengths of $E_0 = 1$, 2 and 4 kV/cm. The crystal parameters employed are the same as those considered in Fig. 2(a). As previously stated, the self-deflection effects are considerably more pronounced at higher values of applied bias strengths as a result of the γ_2 term. Furthermore, for a given value of E_0, this effect depends on r via K_1 and K_2. Figs. 4(a) and 4(b) indicate that these functions reach a maximum in the range $2 < r < 10$. Of course, such behavior should have been anticipated since the intensity FWHM of these optical PR solitons attains a minimum in this region [2,3,7]. The spatial and the angular shifts (analytical and numerical) are also compared in Figs. 6(a) and 6(b) for three different values of r at $E_0 = 2$ kV/cm. Clearly, the two approaches are in good agreement with each other and the small difference between them is attributed to the fact that the evolution of these bright PR solitons is not entirely adiabatic. Nevertheless, this agreement starts to breakdown when soliton decay takes place i.e. at very high bias fields.

In summary, the effects of higher-order electric field terms on the evolution of bright PR solitons have been investigated. By means of numerical methods, we found that these optical solitons experience considerable increase in their self-deflection especially in the high bias field regime. The self-bending process was further studied using perturbation methods. The dependence of the spatial and angular shift on the value of the external electric field was also investigated. We have found that in the high bias field regime the self-deflection follows a cubic polynomial of E_0 whereas in the low bias range it is only linear. The analytical results were then compared to those obtained numerically and were found to be in good agreement with each other.

References

[1] M. Segev, B. Crosignani, A. Yariv and B. Fischer, Phys. Rev. Lett. 68 (1992) 923.
[2] M. Segev, G.C. Valley, B. Crosignani, P. DiPorto and A. Yariv, Phys. Rev. Lett. 73 (1994) 3211.
[3] D.N. Christodoulides and M.I. Carvalho, J. Opt. Soc. Am. B 12 (1995) 1628.
[4] G. Duree, G. Salamo, M. Segev, A. Yariv, B. Crosignani, P.D. Porto and E. Sharp, Optics Lett. 19 (1994) 1195.
[5] M.D. Castillo, P.A. Aguilar, J.J. Mondragon, S. Stepanov and V. Vysloukh, Appl. Phys. Lett. 64 (1994) 408.
[6] M. Shih, M. Segev, G.C. Valley, G. Salamo, B. Crosignani and P. DiPorto, Electron. Lett. 31 (1995) 826.
[7] M.I. Carvalho, S.R. Singh and D.N. Christodoulides, Optics Comm. 120 (1995) 311.
[8] M. Feng Shih, P. Leach, M. Segev, M.H. Garret, G. Salamo and G.C. Valley, Optics Lett. 21 (1995) 324.
[9] R.A. Vazquez, R.R. Neurgaonkar and M.D. Ewbank, J. Opt. Soc. Am. B 9 (1992) 1416.
[10] P. Gunter and J.P. Huignard, Photorefractive Materials and Their Applications I and II, (Springer-Verlag, Berlin, 1988).
[11] V.L. Vinetskii and N. Kukhtarev, Sov. Phys. 16 (1975) 2414.
[12] Y. Kodama and A. Hasegawa, IEEE J. Quantum Electron. 23 (1987) 510.
[13] K.J. Blow, N.J. Doran and D. Wood, J. Opt. Soc. Am. B 5 (1988) 1301.